

Electronic Supporting Information

Pore Volume Regulated CO₂ Adsorption in C-C Bonded Porous Organic Frameworks

Himan Dev Singh,^a Piyush Singh,^a Deepak Rase^a and Ramanathan Vaidhyanathan^{a}*

^aDepartment of Chemistry and Centre for Energy Science,

Indian Institute of Science Education and Research, Dr. Homi Bhabha Road, Pashan,

Pune-411008, Maharashtra-India.

E-mail: vaidhya@iiserpune.ac.in

Table of contents:

1. Materials and methods
2. Analytical characterizations
3. Adsorption studies
4. Rate of adsorption studies

1. Materials and methods

All the chemicals were purchased from sigma aldrich. Triformylphenol, triformylresorcinol, triformylphloroglucinol was synthesized according to previously reported procedure¹ with slight modification.

Synthesis of POF 15:

A solvothermal reaction between 2,4,6-triformylphenol (1 mmol) and pyrrole (2 mmol) in a solution containing 5ml 1,4-dioxane was carried out at 220°C for 48hrs. Black color powder was isolated by filtration and was washed with THF. The air dried sample gave a yield of ~88%. The PXRD pattern indicated this to be amorphous.

Synthesis of POF 16:

A solvothermal reaction between 2,4,6-triformylresorcinol (1 mmol) and pyrrole (2 mmol) in a solution containing 5ml 1,4-dioxane was carried out at 220°C for 48hrs. Black color powder was isolated by filtration and was washed with THF. The air dried sample gave a yield of ~88%. The PXRD pattern indicated this to be amorphous.

Synthesis of POF 17:

A solvothermal reaction between 2,4,6-triformylphloroglucinol (1 mmol) and pyrrole (2 mmol) in a solution containing 5ml 1,4-dioxane was carried out at 220°C for 48hrs. Black color powder was isolated by filtration and was washed with THF. The air dried sample gave a yield of ~88%. The PXRD pattern indicated this to be amorphous.

2. Analytical characterizations

Powder X-ray diffraction:

Powder XRDs were carried out using a Rigaku Miniflex-600 instrument and/or on a Bruker D8 Advance instrument.

Thermogravimetric Analysis (TGA):

Thermogravimetry was carried out on NETSZCH TGA-DSC system. The conventional TGA experiments were done under N₂ gas flow (20 ml min⁻¹) (purge + protective) and samples were heated from RT to 550°C at 2 K min⁻¹.

Infrared spectroscopy:

IR spectra were obtained using a Nicolet ID5 attenuated total reflectance IR spectrometer operating at ambient temperature. The anhydrous KBr pellets were used.

Solid State NMR spectroscopy:

All NMR experiments were carried out on a Bruker Advance NMR spectrometer with a 9.4T

magnet (400.24 MHz proton Larmor frequency, 100.64MHz ^{13}C Larmor frequency) using our probe head for rotors of 4 mm diameter. The parameters for the ^{13}C CP/MAS experiments with TPPM proton decoupling were optimized on glycine, whose carbonyl resonance also served as external, secondary chemical shift standard at 176.06 ppm. For the final ^{13}C CP/MAS NMR spectra up to 600 scans were acquired at 3.1 s recycle delay. The sample was spun at 7.0, 8.0, and 13.3 kHz rotation frequencies to separate isotropic shift peaks and spinning sidebands.

Spinning sidebands are separated from the isotropic shift peak by a multiple of the rotation frequency. The cross-polarization contact time was chosen to be 2.6 ms, which I found previously to be a good compromise between detecting carbons with directly bonded protons and other carbons, for which protons are further removed.

Field Emission-SEM:

Ultra Plus Field Emission Scanning Electron Microscope with integral charge compensator and embedded EsB and AsB detectors. Oxford X-max instruments 80mm². (Carl Zeiss NTS, GmbH), Imaging conditions: 2kV, WD= 2mm, 200kX, InLens detector. For SEM images sample was grind nicely and soaked in MeOH for overnight. Then filtered and dried in hot oven at 80°C. The fine powder was nicely spread over carbon paper and SEM images were taken at different range.

HR-Transmission electron microscopy (HRTEM):

FEI (Jeol FEG 2100F is the model) high-resolution transmission electron microscope (HR-TEM) equipped with a field emission source operating at 300 KeV was used for collecting the TEM images. The well dispersed sample was drop casted on a Cu grid.

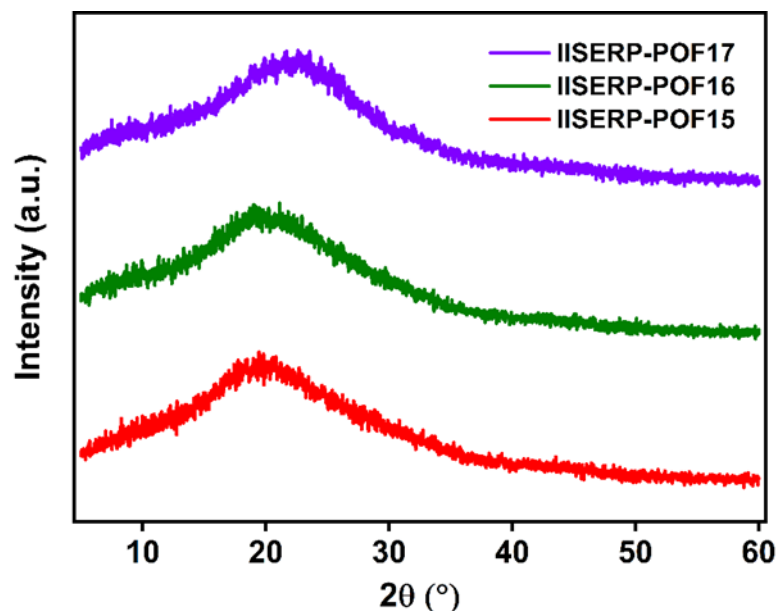


Figure S1. Powder X-ray diffraction patterns of IISERP-POF15,16,17 indicating its amorphous nature.

The big hump at $2\theta = 20^\circ$ is inherent to the polymer. Note: It is not from the glass substrate as plenty of sample was used for the experiment.

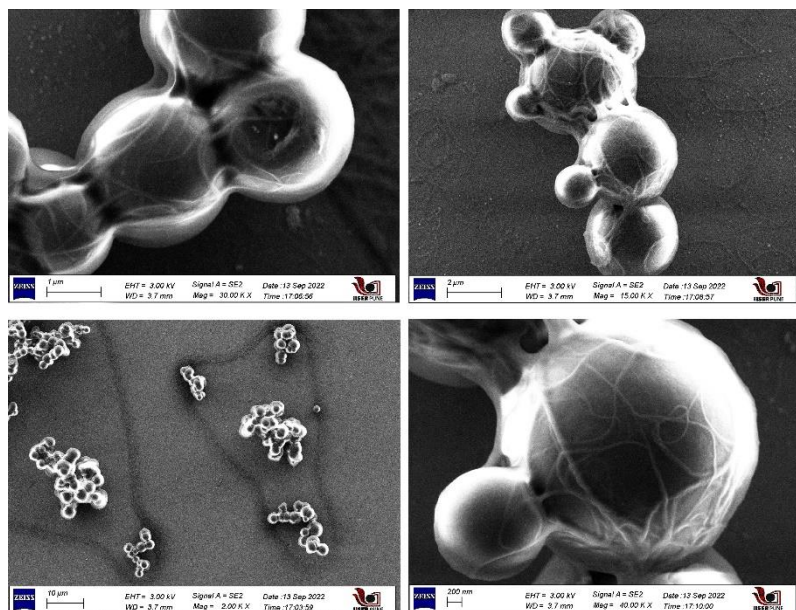


Figure S2. FE-SEM images of IISERP-POF15 microspheres indicating high homogeneity as well as purity of the sample.

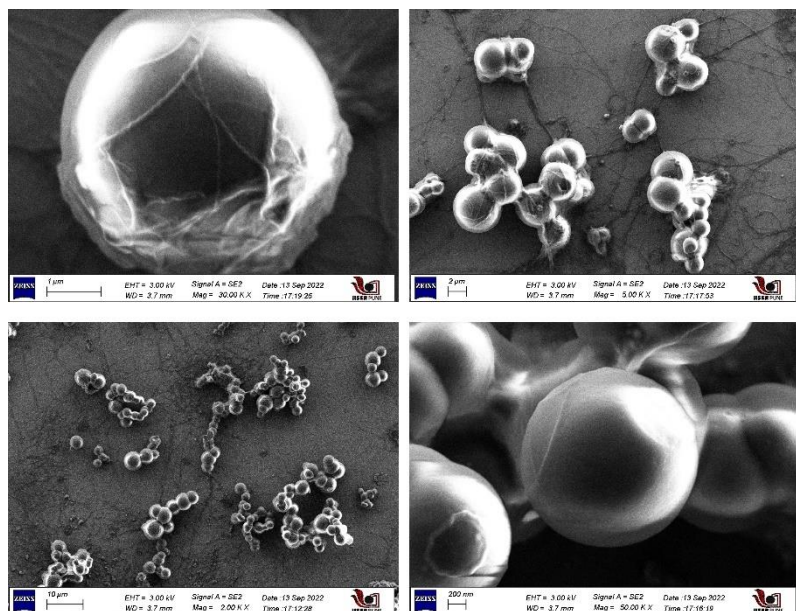


Figure S3. FE-SEM images of IISERP-POF16 microspheres indicating high homogeneity as well as purity of the sample.

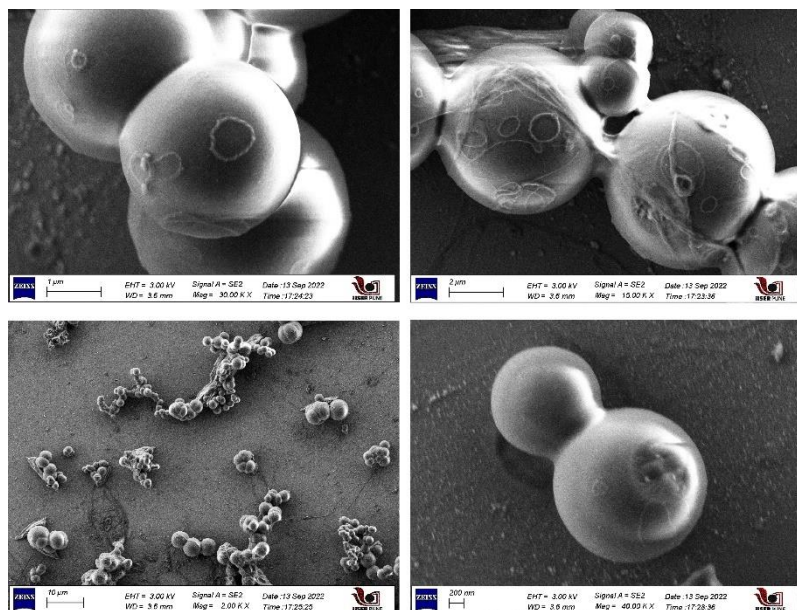


Figure S4. FE-SEM images of IISERP-POF17 microspheres indicating high homogeneity as well as purity of the sample.

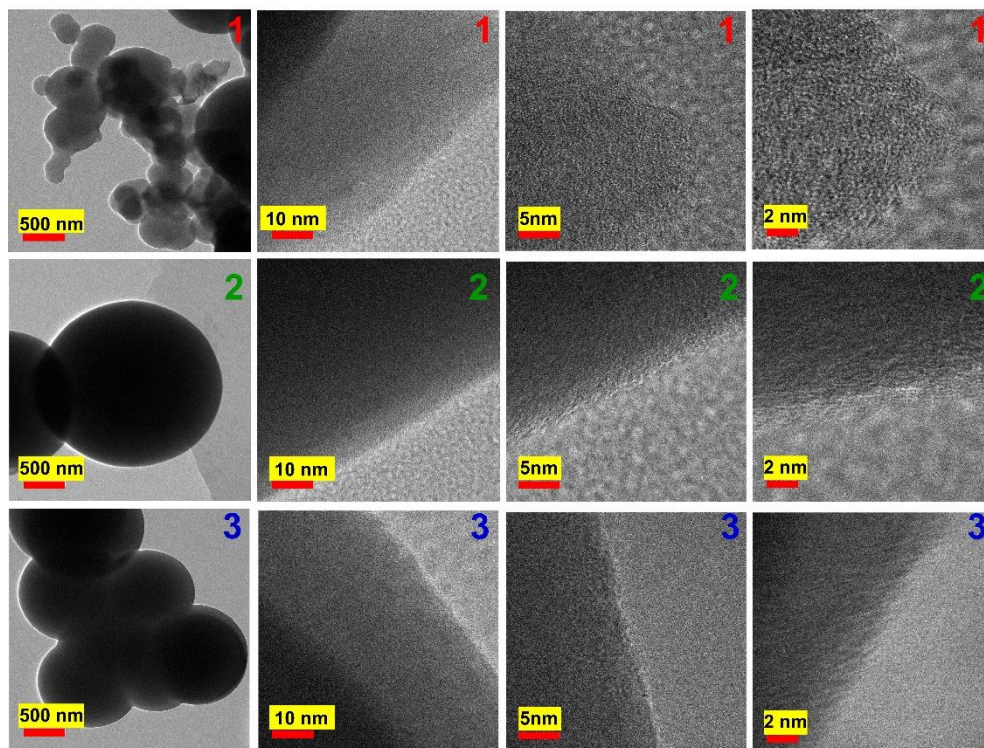


Figure S5. HR-TEM images of POFs showing sphere like morphology and uniform microspheres on the surface.

3. Adsorption studies

All gas sorption isotherms were measured on a Micromeritics ASAP 2020HD instrument using ultra-high purity gases (≥ 4.8 grade). Samples were transferred to a glass tube for

analysis, with dual stage activation: The as-made samples were solvent exchanged by soaking 200mg in 20ml methanol (reagent grade) for 24 hours, with the solvent being replenished every 6hrs. Following this ~ 100mg of the solvent exchanged sample was transferred to analysis glass vial and evacuated at 140°C on the degas port for 16hrs (10^{-6} mbar), at which point the outgas rate was $\leq 2 \mu\text{bar}/\text{min}$.

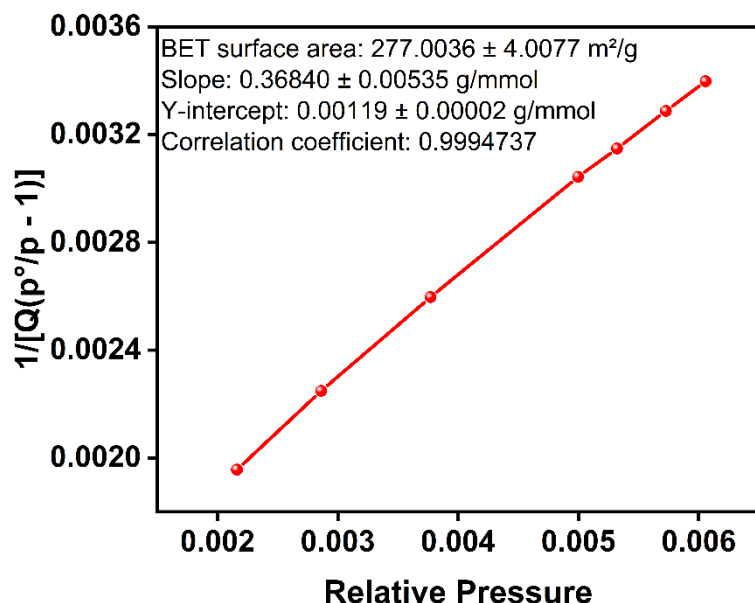


Figure S6. BET fit of IISERP-POF15 from the 273 K CO_2 isotherm.

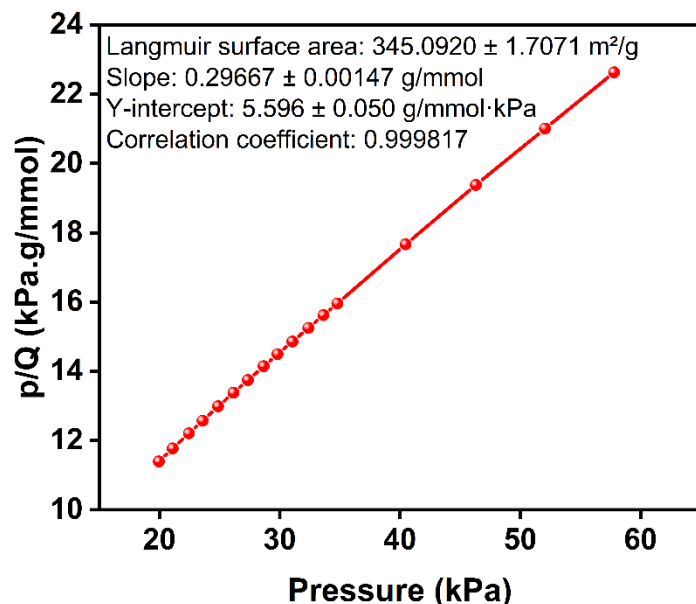


Figure S7. Langmuir fit of IISERP-POF15 from the 273 K CO_2 isotherm.

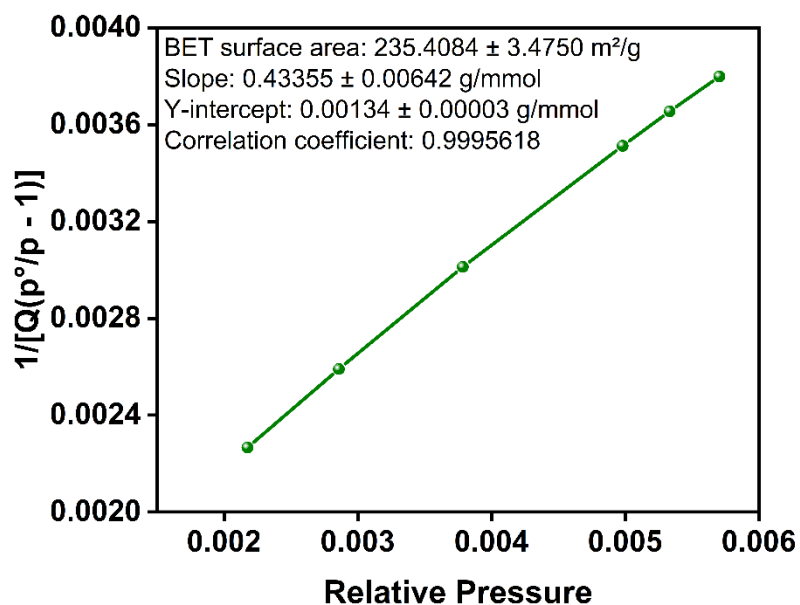


Figure S8. BET fit of IISERP-POF16 from the 273 K CO₂ isotherm.

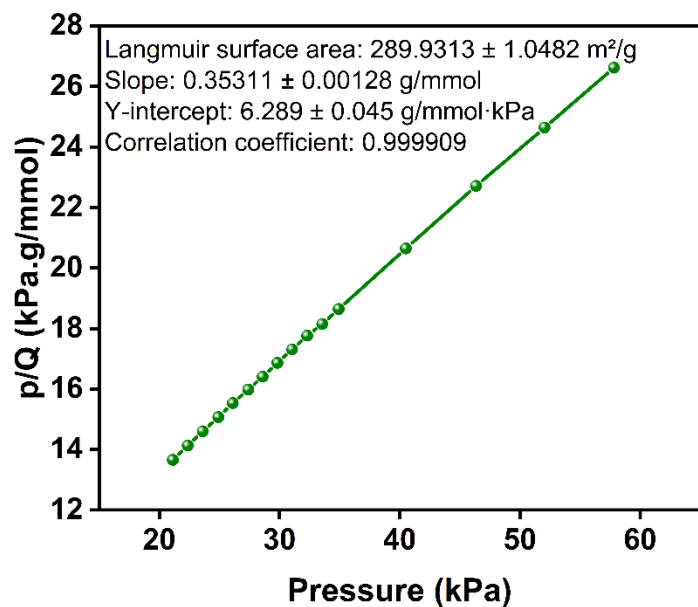


Figure S9. Langmuir fit of IISERP-POF16 from the 273 K CO₂ isotherm.

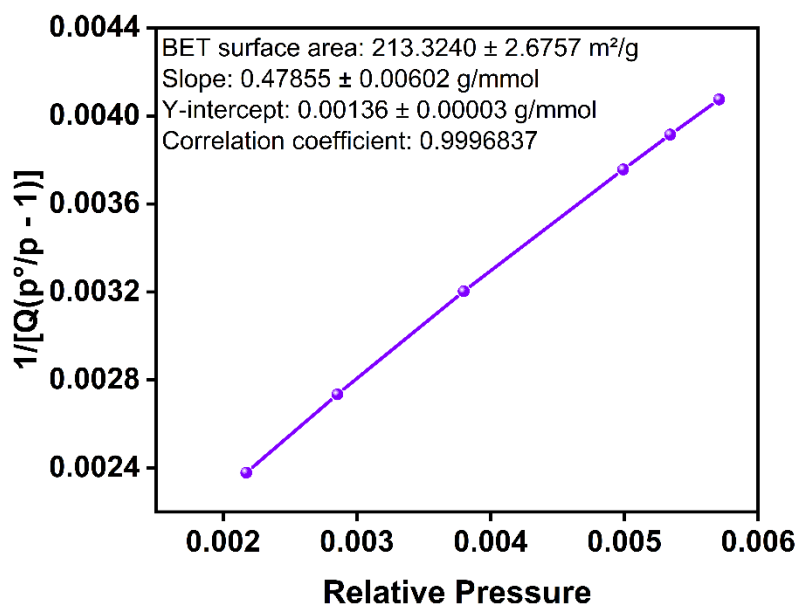


Figure S10. BET fit of IISERP-POF17 from the 273 K CO₂ isotherm.

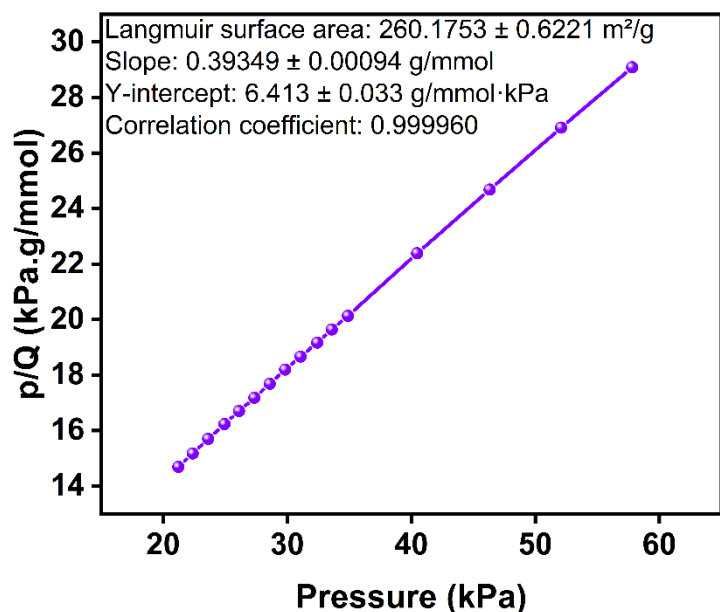


Figure S11. Langmuir fit of IISERP-POF17 from the 273 K CO₂ isotherm.

Virial analysis:

The CO₂ adsorption data were collected from 0-1 bar at 273, 298 and 313 K. For virial fitting the 273, 298 and 313 K isotherms were taken and fitted by the virial equation.

$$\ln(P) = \ln(V_a) + (A_0 + A_1 \cdot V_a + A_2 \cdot V_a^2 \dots + A_6 \cdot V_a^6) / T + (B_0 + B_1 \cdot V_a)$$

Where, P is the pressure during experiment, V_a is amount of gas adsorbed, T is temperature, and A₀, A₁, A₂..., A₄ and B₀, B₁ are temperature independent empirical parameters.

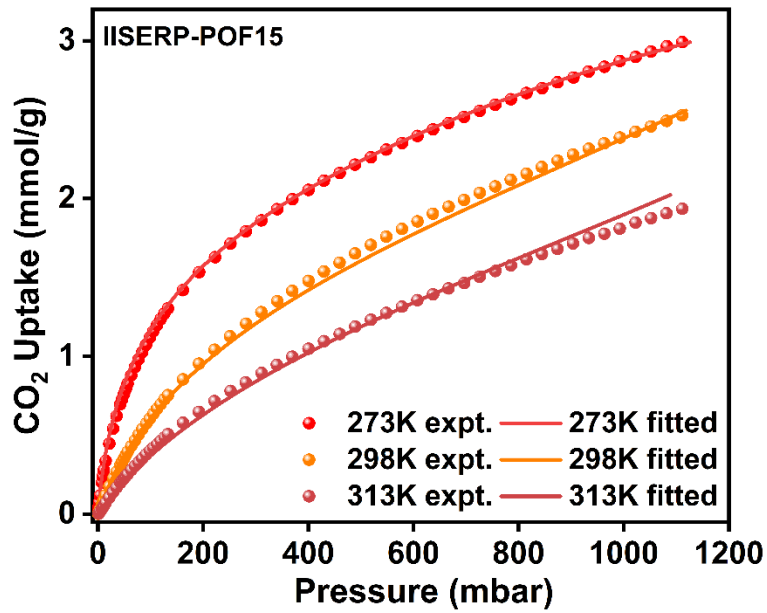


Figure S12. Experimental vs fitted CO₂ isotherm for IISERP-POF15.

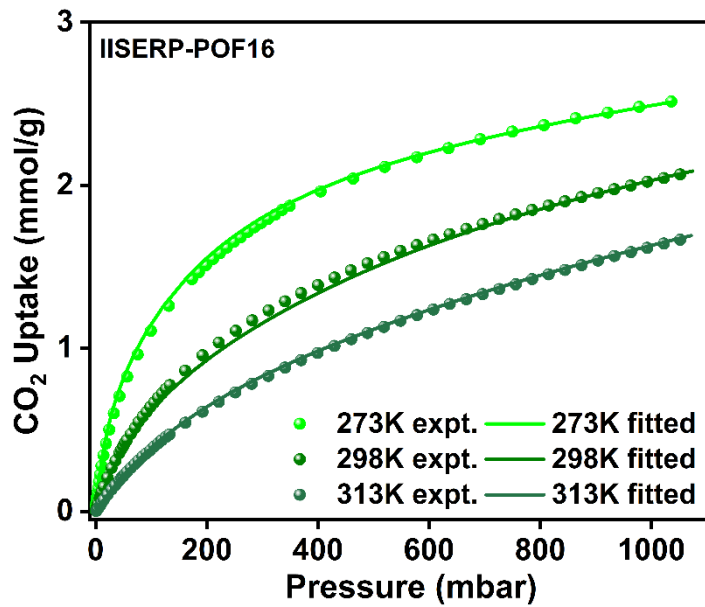


Figure S13. Experimental vs fitted CO₂ isotherm for IISERP-POF16.

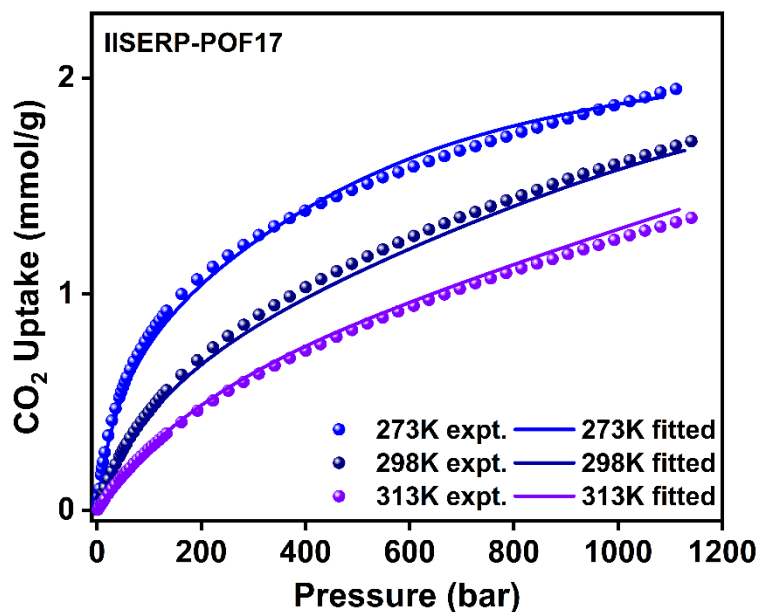


Figure S14. Experimental vs fitted CO₂ isotherm for IISERP-POF17.

Table S1. Virial fitting parameters for IISERP-POF15, IISERP-POF16, IISERP-POF17.

	A0	A1	A2	A3	A4	A5	A6	B0	B1	B2	B3
IISERP-POF15	-4622.4	930.6	79.0	50.6	-20.2	2.7	0	20.0	-2.1	-0.5	0
IISERP-POF16	-4382.1	793.8	-9.6	-49.8	-56.8	67.0	-11	19.3	-2.0	0.36	0.26
IISERP-POF17	-3818.5	948.8	96.1	251.9	-246.5	68.0	0	17.7	-2.1	-0.5	0

Isotherm Fittings:

The isotherms were fit to the Dual-Site Langmuir (DSL) equation using the IAST++ software.²

$$q_i = q_{m,1} \frac{K_1}{1 + K_1 P} P + q_{m,2} \frac{K_2}{1 + K_2 P} P$$

The selectivity equation involved in calculation is provided below.³

$$S_{1,2} = \frac{q_1/q_2}{p_1/p_2}$$

IAST Fitting parameters:

Table S2. IAST fitting parameters for IISERP-POF15, IISERP-POF16 and IISERP-POF17.

		q1	k1	q2	k2	R ²
IISERP-POF15	CO ₂	1.24114	5.51164	5.93211	0.293645	0.999998
	N ₂	4.76069e-11	1.60214e-10	0.901147	0.125414	0.999836
	CH ₄	0.465369	0.940377	1.35275	0.247163	0.999996
IISERP-POF16	CO ₂	0.958704	7.30844	4.15829	0.542074	0.999998
	N ₂	0.041315	0.59615	1.99047	0.0291635	0.999899
	CH ₄	0.490103	0.728483	2.13442	0.0618287	0.999997
IISERP-POF17	CO ₂	0.719379	8.33957	3.0818	0.455436	0.999994
	N ₂	0.691719	0.0963054	0.00121462	5.09968	0.99979
	CH ₄	1.02807e-14	0.221277	1.62439	0.176266	0.999975

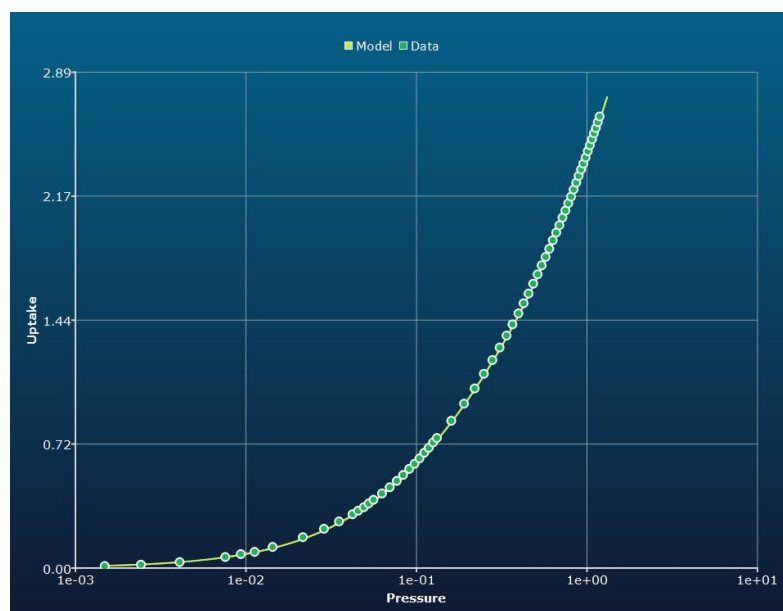


Figure S15. Experimental vs fitted (DSL) CO₂ isotherm for IISERP-POF15.

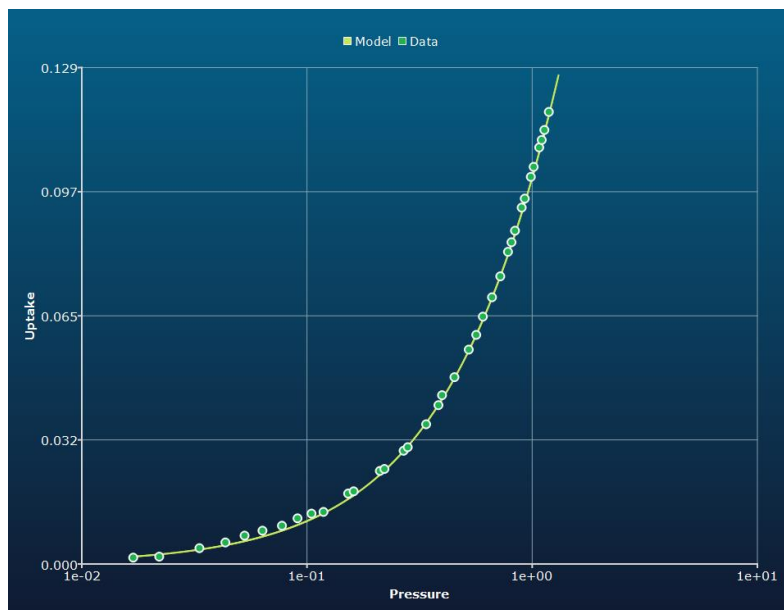


Figure S16. Experimental vs fitted (DSL) N_2 isotherm for IISERP-POF15.

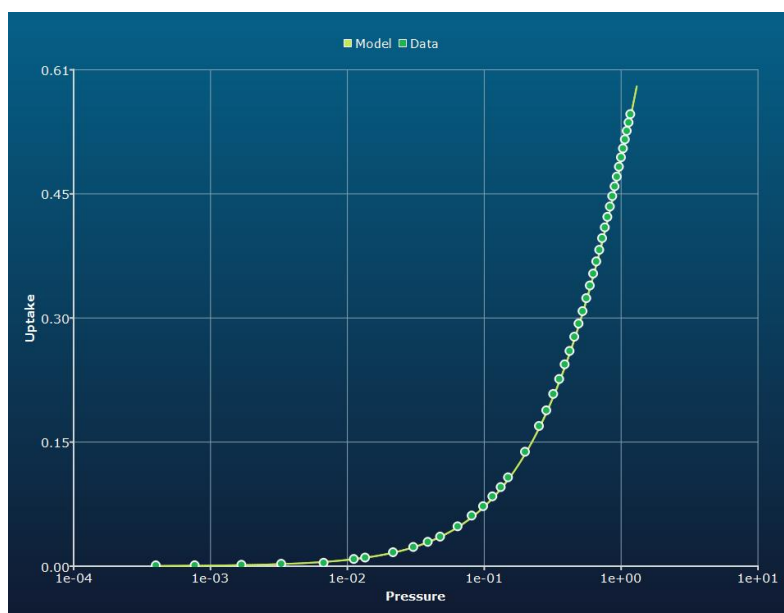


Figure S17. Experimental vs fitted (DSL) CH_4 isotherm for IISERP-POF15.

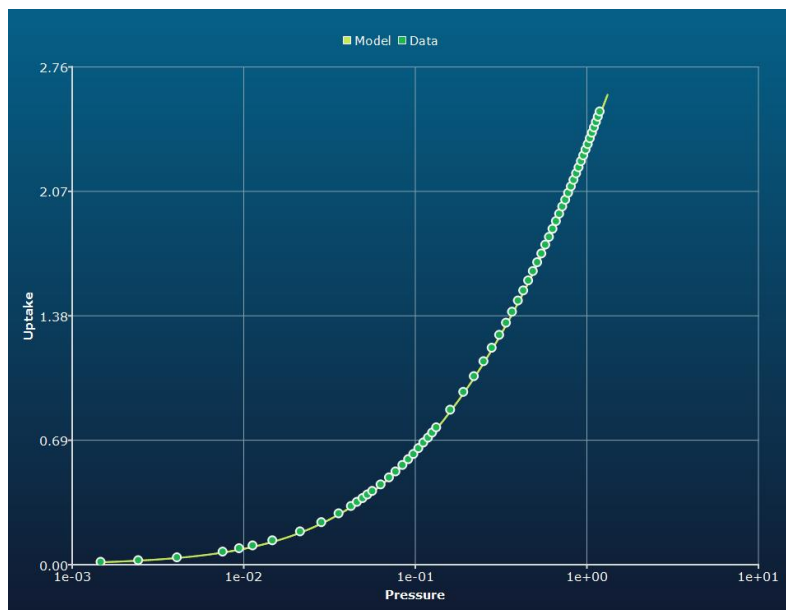


Figure S18. Experimental vs fitted (DSL) CO₂ isotherm for IISERP-POF16.

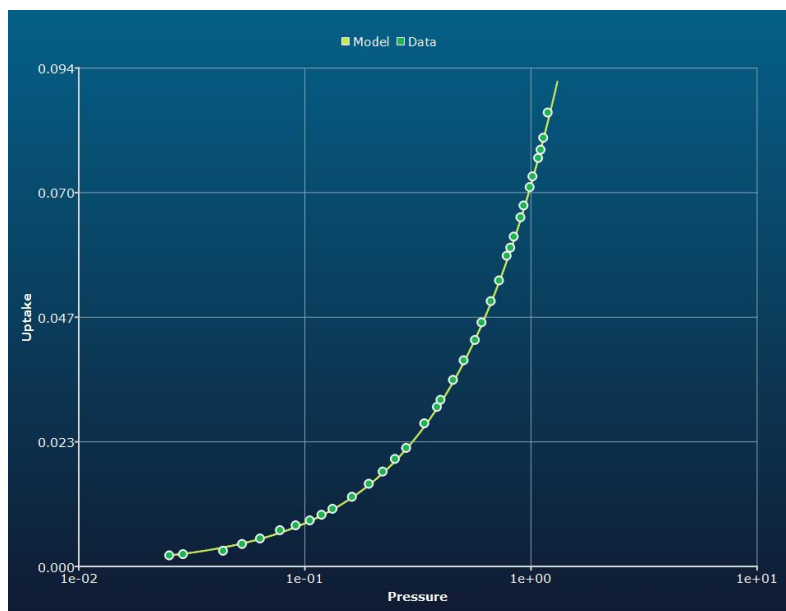


Figure S19. Experimental vs fitted (DSL) N₂ isotherm for IISERP-POF16.

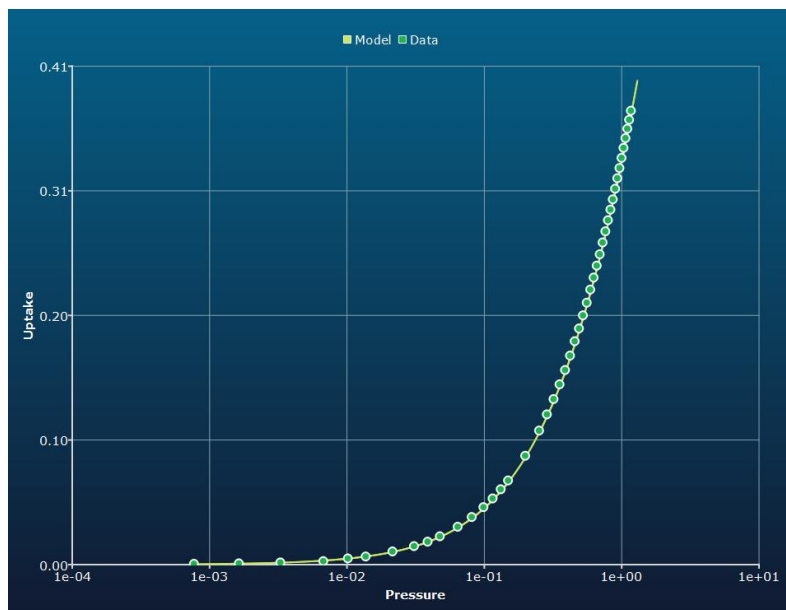


Figure S20. Experimental vs fitted (DSL) CH_4 isotherm for IISERP-POF16.

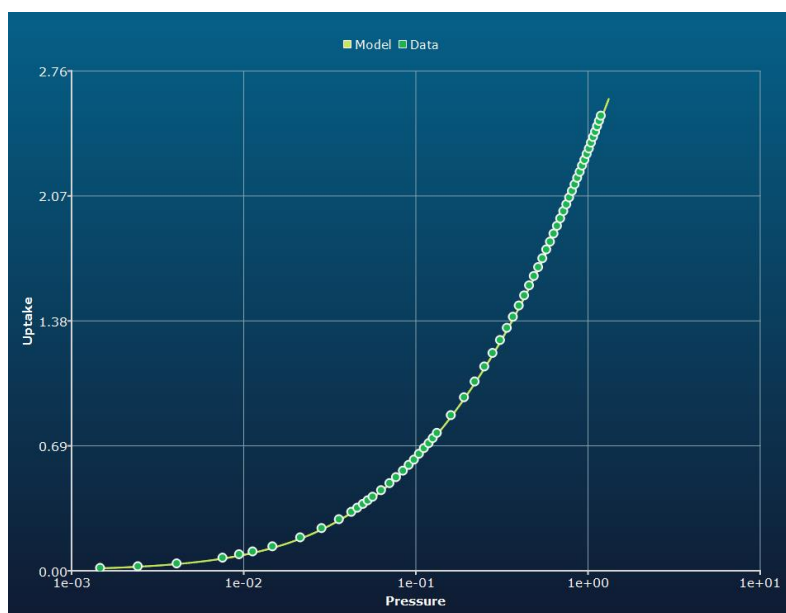


Figure S21. Experimental vs fitted (DSL) CO_2 isotherm for IISERP-POF17.

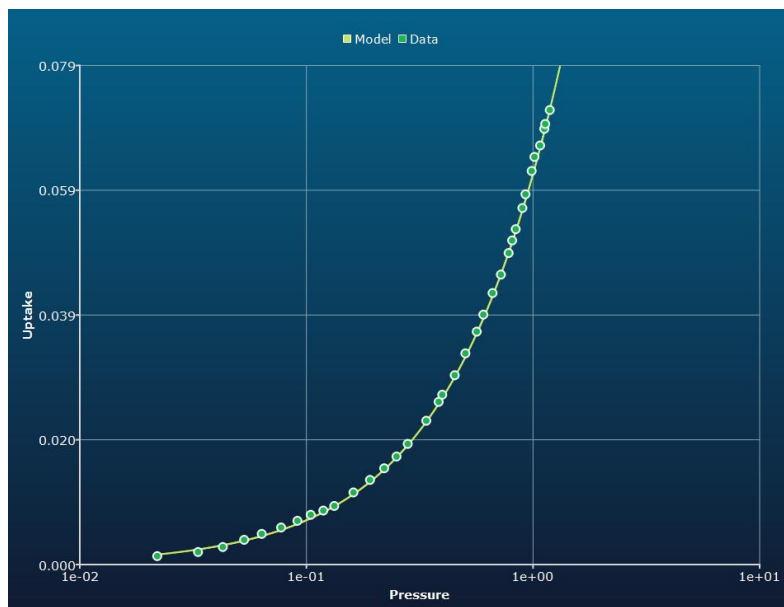


Figure S22. Experimental vs fitted (DSL) N₂ isotherm for IISERP-POF17.

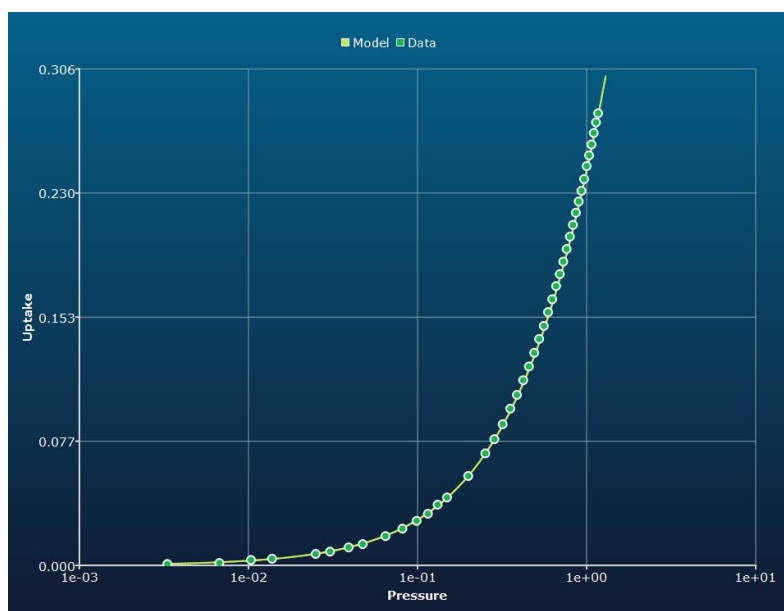


Figure S23. Experimental vs fitted (DSL) CH₄ isotherm for IISERP-POF17.

4. Rate of Adsorption

Diffusion coefficient determination from Rate of Adsorption (ROA) measurements: An extremely high resolution isotherm measurement was carried out using the ASAP2020HD instrument at 273K in the pressure range of 0-1bar. The diffusion coefficient was calculated as a function of CO₂ loading. For this purpose, 8 different loading points were used and each of the ROA data was fitted to a spherical pore model.⁴

$$F = 1 - \frac{6}{\pi^2} \sum_{n=1}^{\infty} \frac{1}{n^2} \text{Exp}(-n^2 \pi^2 \tau)$$

F = fractional uptake; τ = non-dimensional time given by $\tau = Dt/R^2$, where R= particle size; t= time (secs); D = apparent diffusivity

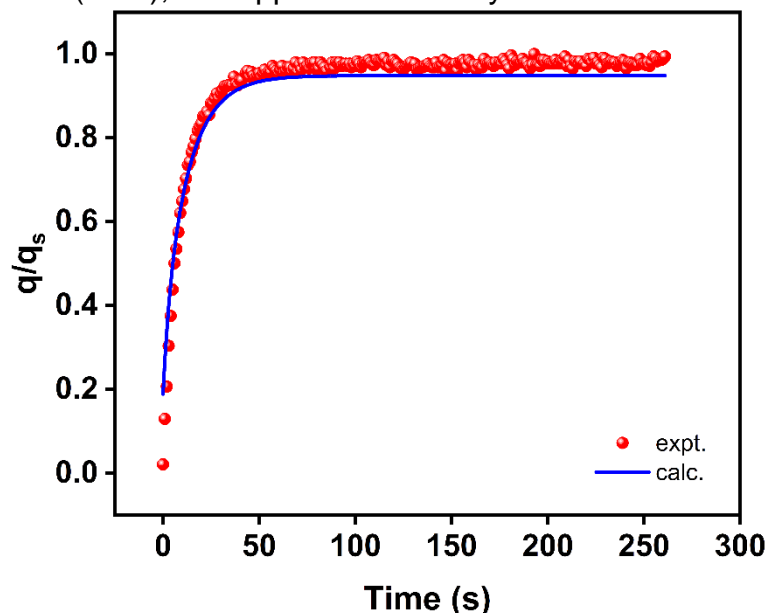


Figure S24. Representative plot of the adsorbate fractional filling vs time showing the fit between the spherical model (line) and the collected data (spheres) obtained from the single component CO₂ isotherm of **1**.

Table S3: CO₂ uptake and CO₂/N₂ selectivity comparison of some of the reported materials.

Sample	CO ₂ Uptake (mmol/g) @273K	CO ₂ /N ₂ Selectivity	Reference
CTF-1	3	20 ^a	Energy Environ. Sci., 2013, 6, 3684–3692
FCTF-1-600	5.53	19 ^a	Energy Environ. Sci., 2013, 6, 3684–3692
F-DCBP-CTF-1	5.98	31 ^c	J. Mater. Chem. A, 2018, 6, 6370–6375
F ₁₂ CTF-3	6.58	32.4 ^c	J. Mater. Chem. A, 2019, 7, 17277–17282
HAT-CTF-450/600	6.3	160 ^c	J. Am. Chem. Soc., 2016, 138, 11497–11500
Isox-CTF-5-400	4.92	29 ^c	Chem. – Eur. J., 2020, 26, 1548–1557
CTF-CSU38	2.2	72 ^b	ACS Appl. Mater. Interfaces, 2018, 10, 36002–36009
CQN-1g	7.16	42.7 ^a	Angew. Chem., Int. Ed., 2019, 58, 872–876

Th-1	2.88	39 ^c	Adv. Mater., 2012, 24, 5703–5707
Py-1	2.71	117 ^c	Adv. Mater., 2012, 24, 5703–5707
Fu-1	2.21	50 ^c	Adv. Mater., 2012, 24, 5703–5707
HMC-3	7.1	23 ^c	ACS Sustain. Chem. Eng., 2016, 4, 3697–3703
Tp-POP1	0.75	30.1 ^c	ACS Appl. Nano Mater., 2022, 5, 5302–5315
TAP3	3.4	114 ^c	ACS Appl. Polym. Mater., 2019, 1, 959–968
TBOSBL1	4	68 ^c	ACS Omega, 2020, 5, 4250–4260
ZNJU-26	3.06 [*]	37.3 ^b	Inorg. Chem. 2021, 60, 2704–2715
IISERP-POF15	3.08	98 ^b	This Work
IISERP-POF16	2.56	222 ^b	This Work
IISERP-POF17	2.0	171 ^b	This Work

a = IAST (10 CO₂ : 90 N₂), b = IAST (15 CO₂ : 85 N₂), c = Henry's selectivity, * T = 298K.

References:

1. S. Haldar, R. Kushwaha, R. Maity, and R. Vaidhyanathan, *ACS Materials Lett.* 2019, **1**, 490–497.
2. S. Lee, J. H. Lee and J. Kim, *Korean J. Chem. Eng.*, 2018, **35**, 214-221.
3. Myers, A. L.; Prausnitz, J. M. *AIChE J.* 1965, **11**, 121–127.
4. K. Malek and M.-O. Coppensa, *J. Chem. Phys.*, 2003, **119**, 2801-2811.